Particle Image Velocity Measurements of Undular and Hydraulic Jumps

J. M. Lennon[1] and D. F. Hill[2]

Abstract: Measurements of the mean and turbulent flow fields in undular and hydraulic jumps have been acquired with single-camera particle image velocimetry (PIV). Three Froude numbers, ranging from 1.4 to 3.0, were studied, and in each case data were collected at numerous streamwise locations. The data from these streamwise locations were subsequently compiled into spatially dense (~80,000 grid points) "mosaic" images encompassing both the supercritical and subcritical portions of the flow. The measured mean and turbulent velocity fields provide more detailed views inside undular and hydraulic jumps than were previously available from studies using pointwise measurement techniques. The two-dimensional spatial density of the measurements provides for the determination of gradient-based quantities such as vorticity. The potential for determining boundary shear stress from the velocity data is evaluated with several methodologies. The results are found to be consistent with recent measurements made using Preston tubes. Discussion of the technical aspects of and difficulties involved with applying PIV to hydraulic jumps is provided. These challenges included the identification and tracking of the free surface through image analysis and the scattering of laser light by entrained air bubbles in the roller region.

DOI: 10.1061/(ASCE)0733-9429(2006)132:12(1283)

CE Database subject headings: Hydraulic jumps; Shear stress; Open channel flow; Turbulence; Velocity; Wave measurement.

Introduction

Scientific and engineering interest in hydraulic jumps has been sustained over the past several decades due to the prevalence of jumps in natural and engineered open channel flows. Continually evolving technology has allowed for more sophisticated laboratory studies of jumps, thereby allowing for greater and greater access to the details of the mean and turbulent velocity fields in the supercritical, roller, and subcritical regions of a jump.

Laboratory efforts associated with hydraulic jumps can be loosely categorized depending upon the type of information being sought. For example, many studies have considered the effects of inflow and channel aspect ratio on the structure of the jump. Ohtsu et al. (2001), in their study of inflow effects, developed diagrams delineating the boundary between undular and hydraulic jumps in terms of Froude number and boundary layer development. Similarly, Chanson and Montes (1995) and Ohtsu et al. (2003) sought to classify undular jumps based upon Froude number and cross-sectional aspect ratio.

A second major thrust area in the literature is concerned with the characteristics of air entrainment in hydraulic jumps. For example, Resch et al. (1974) used hot-film anemometry to determine the distributions of void ratio and bubble size in jumps. Chanson and Brattberg (2000) performed similar experiments with a conductivity probe, and, most recently, Murzyn et al. (2005) used an optical probe to determine the distributions of bubble characteristics.

Finally, a major component of hydraulic jump research has traditionally focused on the study of the characteristics of the fluid velocity field. Rouse et al. (1958) are often credited with performing the first detailed measurements of the velocity structure in hydraulic jumps. However, their hot-wire measurements were actually of a confined air flow in a duct shaped to resemble a typical jump profile. The difference in boundary conditions between the "free surface" of their laboratory experiment and that of an actual water jump suggest that their velocity measurements may also differ from those of an actual jump. Rajaratnam (1965) considered velocity measurements of an actual jump, but his instrumentation, a pitot tube, limited the measurements to mean velocity characteristics away from the roller region. The same is true for Leutheusser and Kartha (1972), who used a pitot-static tube to measure mean velocity and a Preston tube to measure boundary shear stress.

Measurements of the turbulent velocity characteristics were performed by Long et al. (1990). They used a laser Doppler anemometer (LDA) to measure submerged hydraulic jumps over a wide range of Froude numbers and submergence factors. The submerged nature of the jumps avoided air entrainment and the related experimental difficulty associated with two-phase flow. For each jump condition, vertical profiles were measured at approximately 10 streamwise locations. The mean velocity data in the fully developed region were compared favorably against classical wall-jet theory. Likewise, the profiles of turbulence intensity and Reynolds stress were found to resemble those of a wall-jet.

The first application of particle image velocimetry (PIV) to moving hydraulic jumps was performed by Hornung et al. (1995). Motivated primarily by the question of vorticity generation in

[1]Water Resources Engineer, PB Water, 100 South Charles St., Baltimore, MD 21201. E-mail: lennonj@pbworld.com

[2]Associate Professor of Civil Engineering, Dept. of Civil and Environmental Engineering, Pennsylvania State Univ., 212 Sackett Building, University Park, PA 16802. E-mail: dfh4@psu.edu

Note. Discussion open until May 1, 2007. Separate discussions must be submitted for individual papers. To extend the closing date by one month, a written request must be filed with the ASCE Managing Editor. The manuscript for this paper was submitted for review and possible publication on November 5, 2004; approved on November 17, 2005. This paper is part of the ***Journal of Hydraulic Engineering***, Vol. 132, No. 12, December 1, 2006. ©ASCE, ISSN 0733-9429/2006/12-1283–1294/ $25.00.

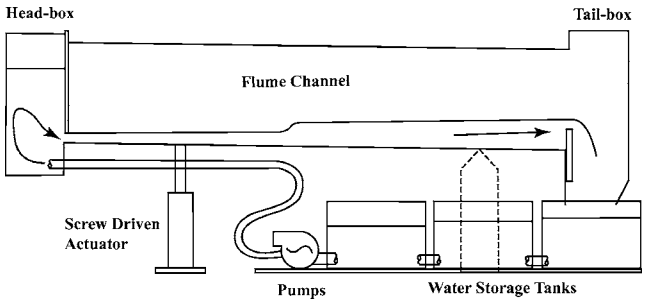

Fig. 1. Schematic representation of experimental flume

hydraulic jumps, their work yielded a spatially dense (grid spacing of 1.6 mm) look at the unsteady flow induced by a passing bore. Their measurements were used to verify a simple control volume analysis of the angular momentum balance in the flow. Due to the unsteady nature of their experiment, it was not possible to obtain large ensembles of data at each stage of the flow. More recently, Misra et al. (2005) conducted PIV studies of a weak hydraulic jump as a model for gently spilling breakers in the surf zone. Their measurements focus on the roller region and present contour plots of mean and turbulent velocity components.

The most comprehensive study to date of the turbulent flow, particularly turbulent stresses, in stationary hydraulic jumps has been performed by Svendsen et al. (2000). Their study used laser Doppler velocimetry (LDV) and specifically focused on weak hydraulic jumps in a flume of 30 cm width. The restriction to low Froude numbers in this study, and in that of Misra et al. (2005), was driven by the motivation to approximate spilling breakers. A side benefit of this restriction to weak jumps is the lack of significant aeration. Bubbles adversely affect hot-film, optical, and acoustic methods and have been a serious impediment to the study of high Froude number free jumps.

Finally, acoustical methods have recently been applied to hydraulic jumps by Liu et al. (2004). While acoustic Doppler velocimetry (ADV) is a less precise technology than LDV, owing to its intrusive nature and larger measurement volume, it benefits from its low cost and ease of use. The measurements of Liu et al. (2004) were used to investigate the spatial distribution of turbulent kinetic energy, Reynolds stress, and turbulence microscale.

The present paper discusses recent PIV measurements of the velocity fields within stationary, free hydraulic jumps. Contrasted with ADV methods, PIV proves to be considerably more (by a factor of 10) expensive, but much more highly resolved. Measurements were made for three Froude numbers in the range of 1.4–3.0. For each Froude number, ensembles of image pairs were collected at ~10 streamwise locations. In postprocessing, the velocity data were compiled into tiled mosaic images of high aspect ratio. The mean and turbulent velocity fields therefore provide the most spatially dense data to date on the flow structure in hydraulic jumps. The data are used to estimate boundary shear stress using a number of methodologies. The results suggest that, given adequate optical access, it is possible to use PIV measurements to determine such stresses in complex open channel flows.

Experimental Investigation

Facilities and Instrumentation

Experiments were performed in a tilting recirculating flume having a length of 4.9 m and a width b of 0.3 m, shown schematically in Fig. 1. The strength and location of the free jumps were controlled with a sluice, or "head," gate and a tail gate, both of which were thin, rectangular plates controlled by motor-driven actuators. Water was recirculated via two centrifugal pumps that provided a total flow rate of nominally 6.4 liters per second (Lps). Initial trials revealed cross-channel variability in the flow as it emerged from underneath the sluice gate. In an effort to provide as smooth and laterally uniform an initial flow as possible, a 30 cm length of flow straightener was positioned immediately downstream of the sluice gate. This straightener spanned the width of the channel and the depth of the flow and was made of 0.64-cm-diameter honeycomb material from Plascore, Inc.

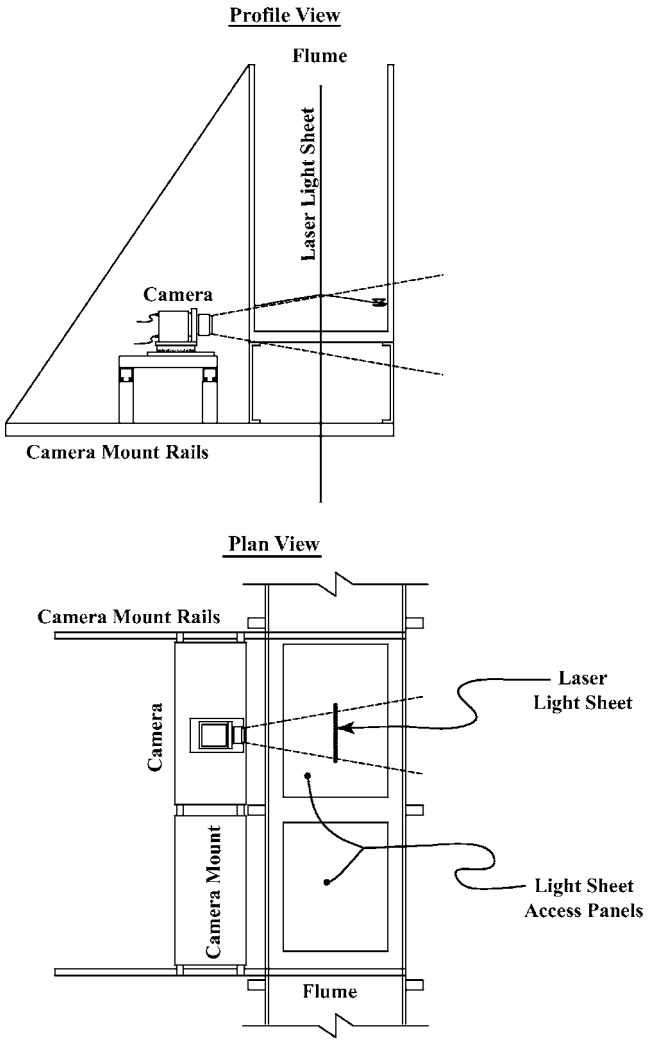

Fig. 2. Plan and profile views of the test section of the present experiments. The views show the relative orientations of the camera and laser light sheet. Note also the "gap" between the acrylic panels in the flume bottom.

Velocity measurements were made with a PIV system from TSI, Inc., that consisted of a 12-bit 4 megapixel camera, double-pulsed 120 mJ Nd:Yag lasers, a synchronizer, and acquisition software. To introduce a vertical light sheet, coincident with the centerline of the flume, the laser was positioned horizontally beneath the flume. A stainless steel (#7 finish) mirror was used to redirect the sheet vertically up through acrylic access panels in the flume bottom. Detailed plan and profile views of the test section of the flume are provided in Fig. 2. The camera was mounted on rails parallel to the flume, allowing for rapid and accurate

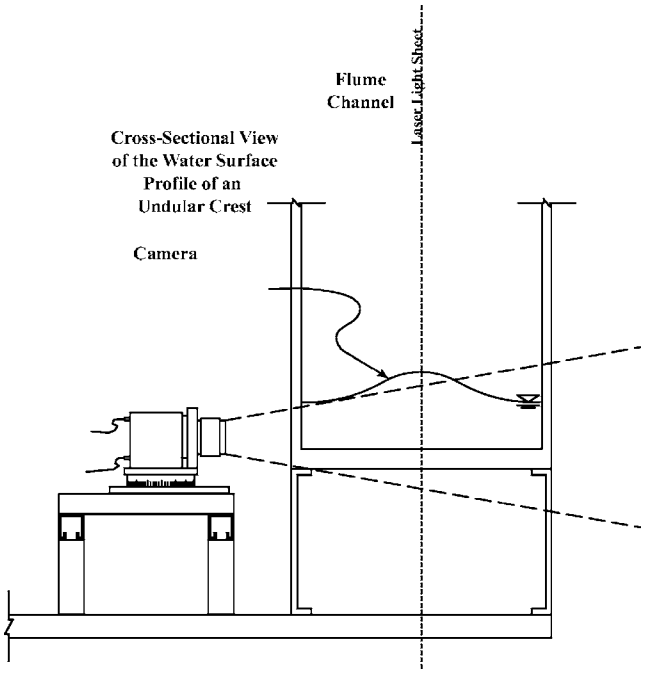

Fig. 3. Schematic of obscured crest region in the case of an undular jump. This obstruction prevents the acquisition of PIV data in the region immediately below the crest.

positioning in the streamwise and lateral directions. Vertical positioning of the camera was facilitated through the use of spacer blocks.

Optical access for the laser light sheet was provided by two acrylic panels in the bottom of the flume. The two panels were separated from each other by a structural support member. With the assumption of a fully-developed supercritical inflow, the most interesting flow regions of a hydraulic jump are at and downstream of the roller. Therefore, the jumps in the present study were adjusted so that the roller was positioned roughly over the middle of the upstream acrylic panel. This maximized the length of subcritical flow available for data acquisition. Nevertheless, regions of missing data, or "holes," due to the obstruction of the laser light sheet by the structural member were seen in all of the results.

Holes in the data also occurred in the region of the first crest of undular jumps. As has been extensively documented (Montes and Chanson, 1998; Ohtsu et al. 2003), undular jumps can demonstrate significant cross-channel variations in free-surface elevation. As illustrated in Fig. 3, this can obscure the optical path of a horizontally mounted camera trying to access the flow directly underneath the crest.

Given the large aspect ratio (length to depth) of the jumps, it was necessary to acquire data at numerous streamwise locations. This is qualitatively illustrated in Fig. 4. Adjacent fields of view were slightly overlapped in an effort to minimize gaps between the ensemble-averaged fields. These gaps can arise due to poor correlations at the edges of the images, which in turn are due to the relatively dim illumination at the edges of the laser light sheet.

For the lower Froude number experiments, where air entrainment at the roller was not significant, the flow was seeded with $\sim$10 μm diameter Sphericel (Potters Industries) hollow glass spheres. gravity of 1.1, these particles work well for many standard PIV applications in water flows. In the highest Froude number experiment, however, the significant entrainment of large air bubbles precluded the use of standard particles. This is because the camera aperture settings that individually optimized the images of the seed particles and prevented charge-coupled device (CCD) array damage from the bubbles were too widely separated. To circumvent this experimental difficulty, fluorescent particles and a camera filter were used. The particles were coated with Rhodamine dye, with a peak emission wavelength of 572 cm. The camera was equipped with a standard #22 orange-red longpass filter with a central wavelength of 560 cm. This combination of particles and filter proved successful in screening out the harmful bubble reflections while transmitting seed particles images.

Finally, the water depth was determined using a variety of methodologies. While initial plans called for the use of a standard surface-piercing capacitance wave gauge, this proved to be unreliable for the lower Froude numbers studied. This is because, despite its extremely small cross section, the disturbance that the wire and its support bracket induced was sufficient to move the weaker jumps upstream. As a result, surface elevation measurements were made in this fashion only for the strongest Froude number studied. For the other jumps, rough elevation measurements were made with a standard point gauge. Finally, and as will be discussed in the following section, determination of the free surface location through image analysis was also attempted, with some success.

Procedures and Analysis

The present measurements include hydraulic jumps at three different Froude numbers. For each of the three trials, velocity data

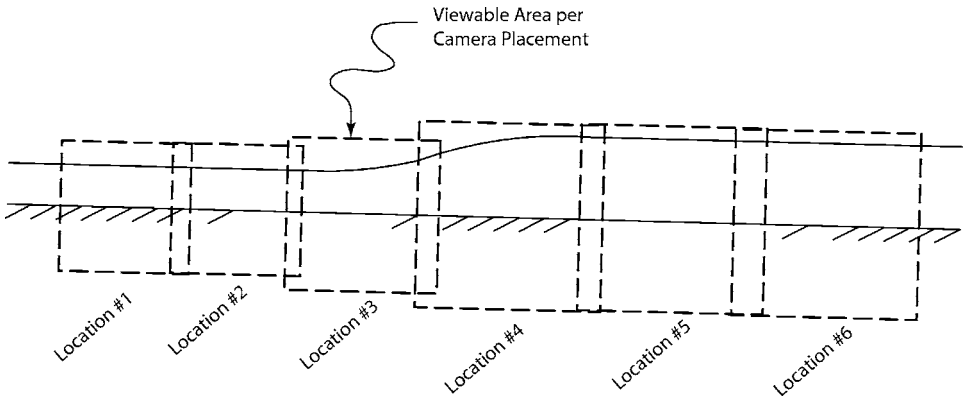

Fig. 4. Schematic of multiple data acquisition areas

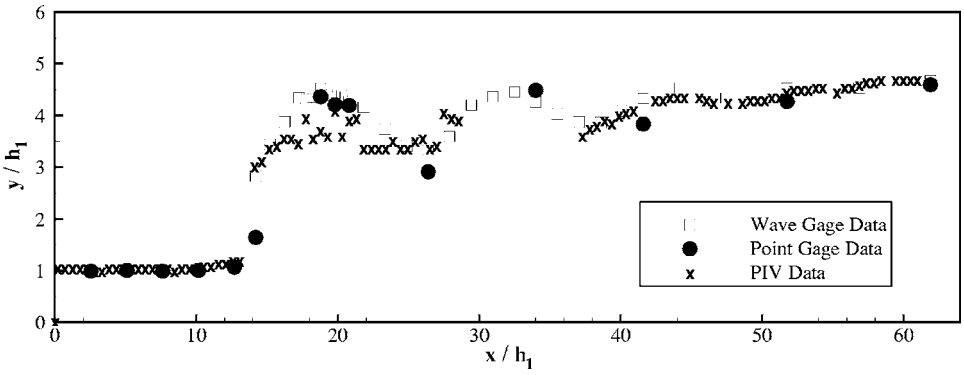

Fig. 5. Nondimensional free surface profile for Trial 3. Profile is taken along the centerline of the flume.

were taken at approximately 10 streamwise locations. At each location, an ensemble of 400 image pairs was acquired with the PIV system. The image pairs were subsequently interrogated and validated using PIVSleuth Christensen et al. 2000 and CleanVec, both developed at the Laboratory for Turbulence and Complex Flow at the University of Illinois. The window size in PIVSleuth was, in all cases, set to 32×32 pixels and a 50% overlap was used. While the exact resolution varied from streamwise location to location (finer for the supercritical flow region), a nominal average value is 20 pixel mm^{-1}. Thus, vector grid spacing of 0.75 mm was fairly typical.

The validation algorithms routinely removed between 1 and 10% of the raw vectors. However, the data quality was much higher than these numbers suggest. While PIV interrogation programs typically give the user the option to interrogate only an "area of interest," this area is always and necessarily rectangular. In the present experiments, a rectangular area of interest exists only in the supercritical approach flow, where the free surface is horizontal and parallel to the flume bottom. At other streamwise locations (e.g., see Location #4 in Fig. 4), much of the acquisition area is "air," where no data exist. If these nonphysical regions are discounted, the rate of vector removal during validation proves to be extremely small, on the order of 1%.

Indeed, this very principle was exploited in an effort to, during postprocessing, determine the position of the free surface. At each streamwise location, the number of valid (i.e., not removed) vectors at each grid point was tallied during the ensemble averaging. Vertical profiles of the number of valid vectors revealed a generally sharp transition from 400, corresponding to grid points always in water, to zero, corresponding to grid points always in air. The transition region in between was due to small vertical oscillations of the free surface. The application of a suitable threshold—say, 50% valid vectors—will, in principle, locate the mean position of the free surface. As shown in Fig. 5, for the highest Froude number studied, the agreement between this method and the other methods for determining the free surface elevation can be quite good, suggesting its utility as a nonintrusive measurement method. The lack of agreement seen beneath the crest is attributable to the three-dimensional nature of the free surface discussed previously and illustrated in Fig. 3.

Experimental Accuracy

Experimental accuracy in PIV tends to be very good, provided that the experimental parameters (seed particle diameter, interrogation window size, etc.) are well optimized. While no straightforward formula for predicting accuracy exists, some estimates are available from Raffel et al. (1998). Their Monte Carlo simulations suggest that, for a 32×32 interrogation window and particle image diameters of 1–3 pixels, displacement uncertainty is around 0.02–0.04 pixels. For the present experiments, computed mean particle displacements were consistently around 2 pixels, indicating that the uncertainty was on the order of a few percent.

Regarding the free surface measurements, given the gain of the capacitance gauge and the 12 bit data acquisition board used, the uncertainty in the electronic measurements was estimated to be 0.03 mm. At a given location, measurements were taken for 2 min, sampling at 25 Hz, in order to smooth out the turbulent fluctuations in the surface. The point gauge has a resolution of 0.25 mm. In practice, however, the uncertainty of the point gauge measurements is much higher due to the inherent subjectivity that arises from a manual measurement of a fluctuating quantity.

Experimental Results and Discussion

General Characteristics

The basic parameters of the supercritical approach flows for the three trials, including flow depth h_1, hydraulic diameter D_h, depth-averaged flow velocity U_1, and Froude ($\mathsf{F}_1=U_1/\sqrt{gh_1}$) and Reynolds ($\mathsf{R}=U_1D_h/\nu$) numbers, are summarized in Table 1. The upper bound of about 3 on the inflow Froude number was limited by two constraints. First, larger pumps would have been required to achieve Froude numbers much greater than 3. Second, the number of bubbles present in significantly stronger jumps would have been problematic. As discussed previously, it is possible to screen out the reflections due to the bubbles. The problem with very bubbly flows, however, is that the bubbles distort the optical rays between the image and acquisition planes. Despite the relatively short optical path in the present experiments (15 cm from flume sidewall to centerline), a high bubble fraction will blur the images of the illuminated seed particles, resulting in poor image correlations. As such, optical methods such as PIV and LDV will

Table 1. Supercritical Approach Flow Parameters for Three Hydraulic Jumps Studied

Trial	h_1 (cm)	D_h (m)	U_1 (cm s^{-1})	F_1	R
1	3.14	0.104	76.2	1.37	79,000
2	3.08	0.102	90.7	1.65	92,700
3	1.97	0.070	131	2.99	91,500

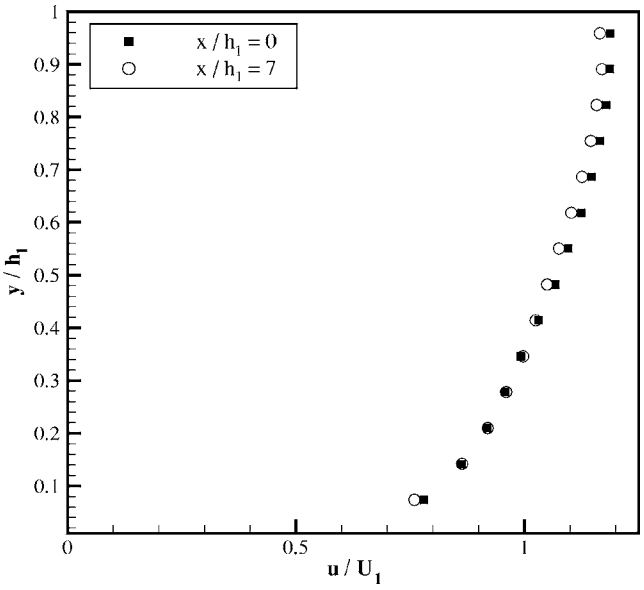

Fig. 6. Vertical profiles of streamwise velocity (Trial 3) at different streamwise locations indicating fully developed nature of flow

have the same difficulties as acoustic and thermal methods when it comes to turbulence measurements in a highly aerated roller.

Regarding the depth-averaged velocity, and quantities such as Reynolds number and Froude number that are based upon it, note that velocity measurements were made only on the flume centerline and therefore did not resolve the lateral velocity gradients in the flow. As a result, the calculations of bulk quantities such as R will be overestimates. The magnitude of this overestimate is anticipated to be only slight, however, given the high cross-sectional aspect ratio ($b/h_1 \sim 10$) of the flow.

To elaborate, the distance from the sluice gate to the test section, approximately 2 m, was just sufficient for the bottom boundary layer to fully develop. This is suggested by the laboratory results of Kirkgoz and Ardichoglu (1997) on open channel flow development lengths. Their results, which discuss development of the vertical boundary layer on the flume centerline, indicate that, for the range of R and F in the present study, entrance lengths of 1.5–2.1 m are expected. The conclusion that the supercritical approach flows in the present experiments were fully developed vertically is further confirmed by considering typical data, as illustrated in Fig. 6. Vertical profiles of streamwise velocity for Trial 3 are presented at two different streamwise locations. The high degree of similarity between the two profiles confirms that the flow is essentially fully developed at the beginning of the acquisition region.

Next, consider the development of the lateral velocity profile. Given the high aspect ratio of the flows in the present experiments, it is anticipated that the effects of the sidewalls on the flow will be fairly minimal. To support this, consider data from Kirkgoz and Ardichoglu (1997) for a test case with the lesser aspect ratio of 4. As with the present experiments, their flume had a width of 30 cm. At a distance of 5 cm away from the sidewall, the measured depth-averaged velocity was the same as that on the flume centerline. At a distance of 3 cm away, the velocity was reduced over the centerline value by only 5%. In summary, therefore, the exclusive focus of the present measurements on centerline quantities will only mildly overestimate parameters such as R and F.

Mean Velocity Data

Ensemble averaged mean velocity data for the three trials are presented in Fig. 7. For each case, a contour plot of the streamwise velocity component and a two-dimensional velocity vector map are presented. Note that velocities have been normalized by U_1 and that distances have been normalized by h_1. Second, for the sake of clarity in the vector maps, only every fifth vector in the vertical and every 35th vector in the horizontal is plotted. This amounts to only ~0.6% of the available vectors being displayed. Third, the plots are all undistorted, so that the true aspect ratios of the jumps are preserved. Finally, recall that the origin in all cases was taken to be the upstream edge of the upstream acrylic panel in the flume bottom.

The contour and vector plots all demonstrate a clear boundary layer structure in the incoming supercritical flow. For the weakest jump studied, there is only a slight disruption to this boundary layer profile throughout the extent of the jump. For the intermediate jump, the subcritical flow is much more wavy in structure, with regions of high velocity in the troughs of the undular profile. The strongest jump studied is the one closest to a classical hydraulic jump. The high velocity inflow deflects upwards underneath the first crest, much like a wall-jet detaching from a boundary. The extremely low velocity underneath the roller region suggests a significant reduction in boundary shear in that area.

Out-of-plane vorticity is easily derived from the mean velocity fields. For the lowest two Froude numbers studied, where rollers were absent, the only significant vorticity was the negative (clockwise) vorticity near the bottom boundary of the flume. In the strongest jump, however, and as illustrated in Fig. 8, positive vorticity was observed in the roller region and in the first trough of the undular flow downstream. For clarity, the free surface is also plotted. As discussed previously, three-dimensional effects and a high bubble fraction prevented full optical access to the roller region, hence the gap in the data in the roller and crest regions.

Turbulent Velocity Data

Similar contour plots of the turbulent velocity fields are readily created from the ensembles. As one example, consider horizontal velocity fluctuations in the roller region from Trial 3, as shown in Fig. 9. In this figure, only the region near the roller has been shown. In the supercritical approach flow, the highest values of u'_{rms}, which are on the order of 10% of the depth-averaged mean velocity, are found near the bottom boundary, due to the boundary shear. In the roller region itself, much higher values of u'_{rms}, on the order of 40% of U_1, are found in close proximity to the free surface. These results are consistent with those of Misra et al. (2005) from their study of a slightly weaker jump.

The vertical distributions of both u'_{rms} and v'_{rms} in the supercritical approach flow and directly underneath the first crest are shown in Fig. 10 for all three trials. For Trial 1, the mildest case, there is very little qualitative difference between the two longitudinal stations. Quantitatively, the turbulent velocities are slightly higher underneath the crest. Trials 2 and 3 display some similarity with each other and significant differences with Trial 1. The profiles of v'_{rms} underneath the crests are now reversed, with higher values nearer the free surface than the bottom. Additionally, the profiles of u'_{rms} show two peaks, one near the free surface and the other near the bottom. Comparison of Figs. 10(b, d and f) reveals that the near-bottom peak in u'_{rms} underneath the crest moves steadily upwards with increasing F. This is a consequence of the

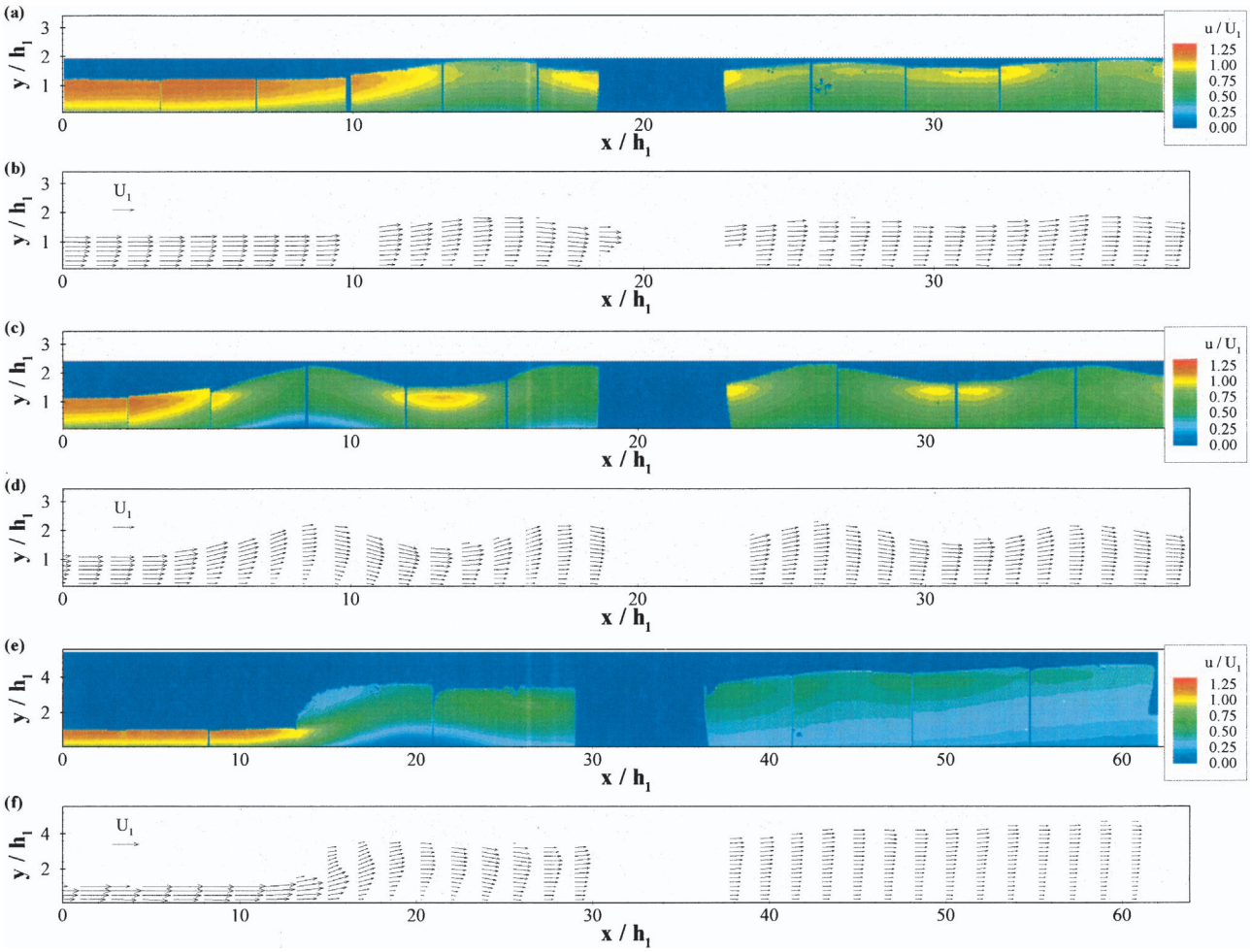

Fig. 7. (Color) Contours of nondimensional streamwise velocity and nondimensional velocity vectors: (a)–(b) Trial 1; (c)–(d) Trial 2; and (e)–(f) Trial 3. For visual clarity, only every fifth vector in the vertical and 35th vector in the horizontal directions is shown.

deflection of the streamwise flow upwards [Figs. 7(c and e)] in this region, which reduces the near-boundary shear production of turbulence.

Shear Stress Determination

An additional goal of the present study is investigating the extent to which mean and turbulent PIV velocity data may be used to estimate boundary shear stress throughout undular and hydraulic jumps. Such information may be of value in terms of predicting the bed-load component of sediment transport occurring beneath jumps in mobile channels. Some previous studies, from the very early (Rajaratnam 1965) to the very recent (Chanson 2000), have used Preston tubes to infer the boundary shear stress. Contrasting the two methods, Preston tubes benefit from their low cost, both initial and operational, and their ease of use. PIV methods, on the other hand, benefit from the spatial density of data inherent to a field measurement method and from the nonintrusive nature of the technique. In the present experiments, because velocity measurements were made solely on the flume centerline, calculations of shear stress will be similarly limited. Other studies, such as Chanson (2000), have reported on the significant variation of boundary stress across the wetted perimeter of the channel.

Uniform Flow Region

In the fully developed supercritical inflow, of course, there are many ways of determining boundary shear:

1. The simplest, perhaps, and one requiring only the flow Reynolds number and boundary roughness information, is to use

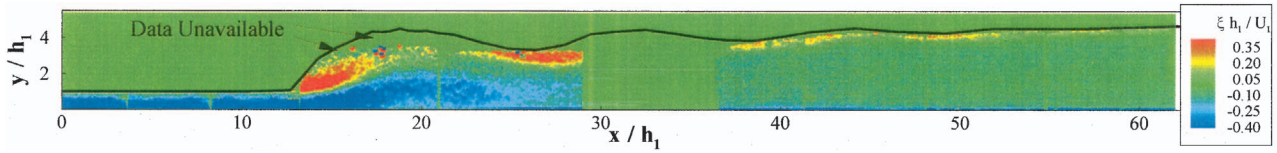

Fig. 8. (Color) Contours of nondimensional out-of-plane vorticity for Trial 3. Note that the lack of optical access in the vicinity of the crest resulted in incomplete imaging of the roller region.

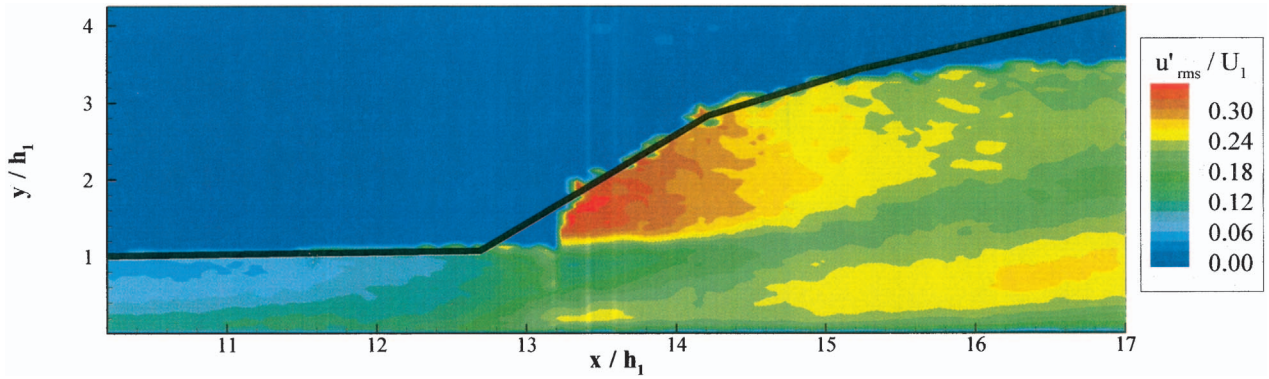

Fig. 9. (Color) Contours of nondimensional values of u'_{rms} for Trial 3. The axes have been zoomed in to focus on the roller region, and the aspect ratio has not been preserved as in the previous figures.

a friction factor approach. Application of the Colebrook-White equation

$$\frac{1}{f^{1/2}} = -2.0\log\left(\frac{\epsilon/D_h}{3.7} + \frac{2.51}{\mathsf{R}_{D_h} f^{1/2}}\right)$$

where ϵ=roughness height, allows for the determination of the friction factor f and hence the boundary shear τ_0. One limitation of this approach is that it necessarily assumes that the shear is uniform over the wetted perimeter. Given the acrylic walls and bottom of the flume, $\epsilon \sim 0$ was assumed for the calculations.

2. Second-order velocity statistics can also be used to estimate shear stress. For the case of uniform flow, Nezu and Rodi (1986) provide the following well-known empirical relations describing the vertical variation of the horizontal and vertical root mean square (rms) velocity fluctuations

$$\frac{u'_{rms}}{u^*} = D_u \exp\left(-\lambda_u \frac{y}{h}\right) \tag{1}$$

$$\frac{v'_{rms}}{u^*} = D_v \exp\left(-\lambda_v \frac{y}{h}\right) \tag{2}$$

where h=flow depth; and $u^* = \sqrt{\tau_0/\rho}$=shear velocity. The constants λ_u and λ_v have been shown to equal 1.0 and 0.67 and the constants D_u and D_v have been shown to equal 2.30 and 1.27. Slight deviations from these universal relations are expected in the viscous layer near the boundary and close to the free surface. For the present measurements, it is straightforward to fit these curves to the data [Figs. 10(a, c and e)], treating the shear velocity as a fitting parameter, in the supercritical approach flow.

3. Finally, knowledge of the Reynolds stresses can be used to deduce shear at the boundary as well. From boundary layer equations, it is straightforward to show that, for uniform flow, the vertical variation of total stress is linear. Over most of the flow depth, the total stress is dominated by the Reynolds stress, due to the weak mean velocity gradients away from the boundary. A linear fit to the Reynolds stress in this outer region can be extrapolated to the boundary in order to determine τ_0. For the present experiments, this is demonstrated in Fig. 11. As shown, the vertical variation of the Reynolds stress in the outer region is indeed linear for the supercritical approach flows of all three trials. Also shown are the vertical profiles underneath the first crests of the three jumps. For Trials 2 and 3, the Reynolds stress becomes negative away from the boundary, indicating the reversal in mean velocity shear seen near the surface. It is clear that, outside of the uniform approach flow, use of boundary layer theory in deducing boundary shear from turbulent stresses is not possible.

A summary of the boundary shear stresses in the approach flows, obtained via these three methods, is provided in Table 2. For Trials 2 and 3, the results are fairly consistent, with coefficients of variation of 10 and 14%, respectively. For Trial 1, it is clear that the results from the velocity fluctuations are at odds with the other two methods. While it is possible that this is a Reynolds number or Froude number effect, adequate data on the variation of the coefficients in Eqs. (1) and (2) with R and F do not exist.

Nonuniform Flow Region

Of greater interest is the assessment of the extent to which PIV data may be used to deduce boundary shear in regions of nonuniform flow. Here, two candidate methods exist: the use of well-known vertical distributions of mean velocity in wall-bounded shear flows and the direct computation of shear from velocity data within the viscous sublayer:

1. Regarding the first method, the application of boundary layer theory to jumps was used by Streinruck et al. (2003) in their theoretical study of turbulent undular jumps. While the logarithmic overlap equation (White 1991) is a popular choice, care must be taken to apply it only in its range of applicability, approximately $30 < y^+ < 300$, where $y^+ = yu^*/\nu$ represents wall units. Montes and Chanson (1998) state that Coles' law of the wake is a superior choice, given that it may be applied throughout the full depth of the flow. Coles' law is given by

$$\frac{u}{u^*} = \frac{1}{\kappa}\log_e(y^+) + B + \frac{2\Pi}{\kappa} f(\eta) \tag{3}$$

In this equation, u=streamwise velocity; and κ and B=near-universal constants, taken to be 0.4 and 5.0, respectively. For rough-wall flows, the second parameter can vary considerably.

The wake parameter Π depends upon the pressure gradient in the flow and can be treated as a free parameter. The wake function $f(\eta)$ is given by

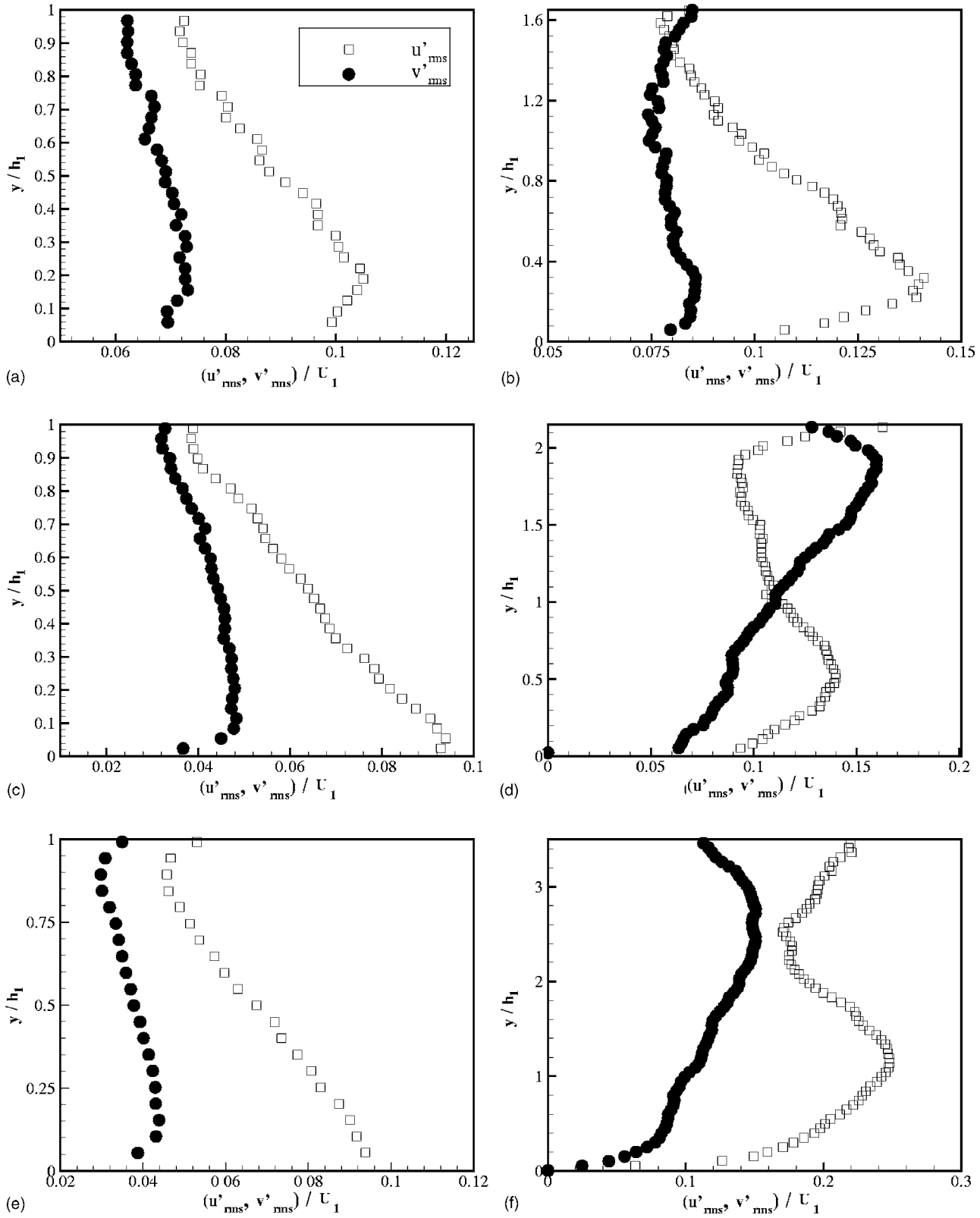

Fig. 10. Vertical profiles of horizontal and vertical turbulent velocities: (a) Trial 1, approach flow; (b) Trial 1, underneath first crest; (c) Trial 2, approach flow; (d) Trial 2, underneath first crest; (e) Trial 3, approach flow; and (f) Trial 3, underneath first crest

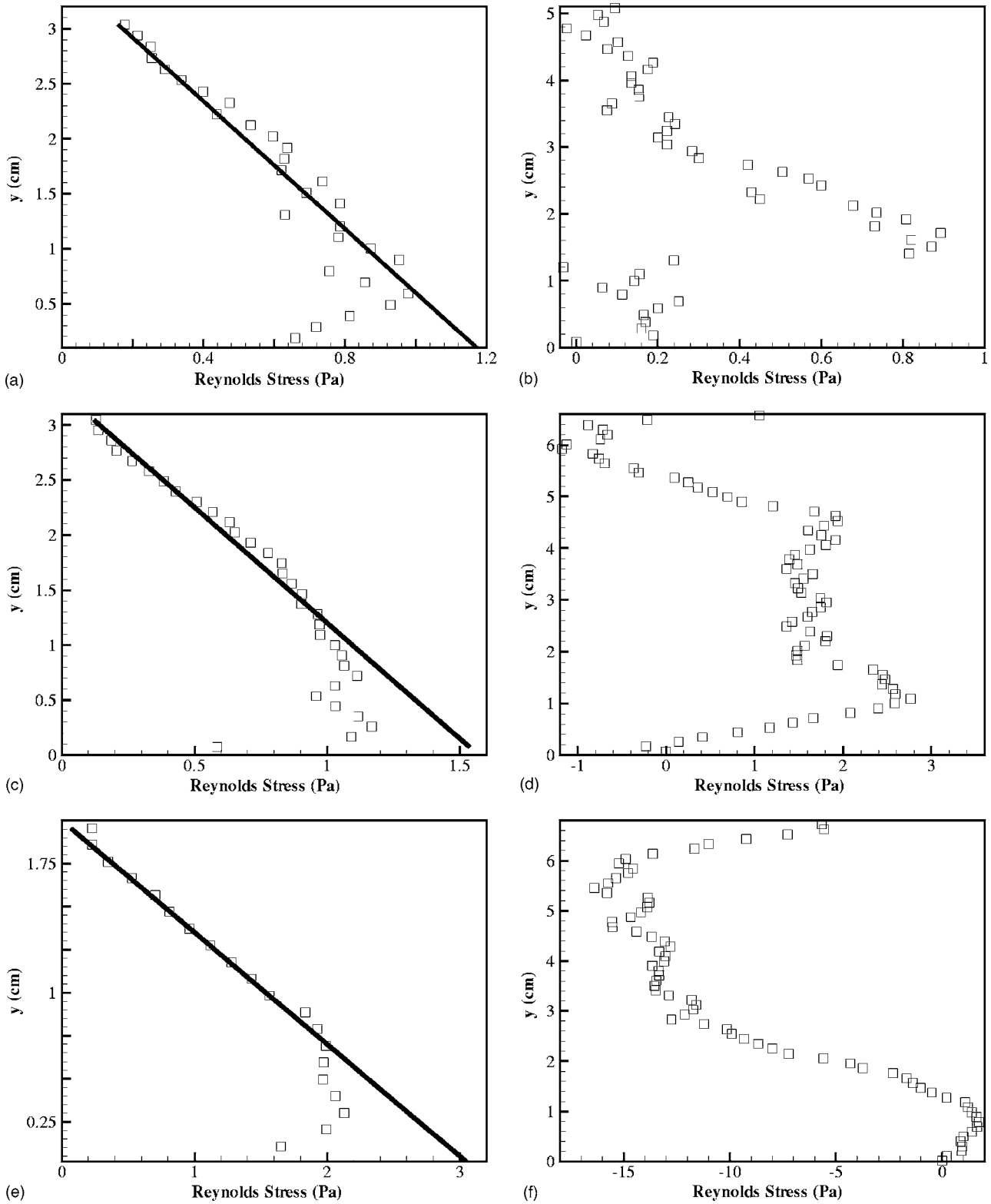

Fig. 11. Vertical profiles of Reynolds stress $-\rho\overline{u'v'}$: (a) Trial 1, approach flow; (b) Trial 1, underneath first crest; (c) Trial 2, approach flow; (d) Trial 2, underneath first crest; (e) Trial 3, approach flow; and (f) Trial 3, underneath first crest

$$f(\eta) = 3\eta^2 - 2\eta^3, \quad \eta = \frac{y}{\delta} \tag{4}$$

where δ=boundary layer thickness. In the fully developed supercritical approach flow, the boundary layer thickness is equal to the flow depth, while in the jump itself, the definition of δ is much less clear. As discussed by White (1991), ambiguity in the definition of δ can lead to a poor agreement between Coles' law and experimental data for nonequilibrium flows. Therefore, the present analysis will fit Coles' law to the data, treating u^*, Π, and δ all as free parameters.

This least-squares analysis was done using Matlab's *fmincon* function, which finds the constrained minimum of a

Table 2. Boundary Shear Stress, in Supercritical Approach Flow Region, as Derived from Colebrook-White Equation, Vertical Distribution of Turbulent Velocities, and Vertical Distribution of Reynolds Stress

Trial	1	2	3
Colebrook-White (Pa)	1.37	1.88	3.96
u'_{rms} (Pa)	2.40	1.65	3.85
v'_{rms} (Pa)	3.29	1.85	2.96
Reynolds stress (Pa)	1.21	1.50	3.08

function of multiple variables. As an example, Fig. 12 shows experimental data and Coles' law for several different velocity profiles. For each of the three trials, velocity profiles in the supercritical approach flow and directly underneath the first crest are considered. In all cases, even beneath the crests, the agreement between the data and the curve fit is extremely good. This suggests that vertical mean velocity profiles throughout the jumps can be used to estimate the boundary shear. The corresponding boundary shear values are summarized in Table 3. Note that the values in the approach flow are in good agreement with those obtained by other methods and that the values beneath the crests are dramatically reduced.

To support the validity of using Coles' law in the present experiments, note first of all that no flow reversal was observed near the boundary. Beneath the crest in Trial 3, the streamwise velocity near the boundary was indeed extremely small, but still positive. Next, Coles (1956) investigates the application of the wake law to the adverse-pressure gradient data of Schubauer and Klebanoff (1950) and others and is able to show excellent agreement between the data and Eq. (3). To do so, Coles (1956) allows u^*, δ, and π to all be smoothly varying functions of streamwise distance x, the precise strategy adopted by the present writers.

2. Turning now to the second method, it is possible to obtain the shear stress directly from velocity measurements within the viscous sublayer. In this constant stress region, generally defined as $y^+ < 5$, the total stress is dominated by the laminar stress, calculated from

$$\tau_{xy} = \mu \frac{\partial u}{\partial y} \tag{5}$$

where μ=dynamic viscosity. In principle, PIV can easily make measurements in the sublayer. In practice, however, the constraint of needing a grid point within the viscous sublayer requires a very high magnification; i.e., the camera must be zoomed in on a very small region close to the boundary. In the present experiments, the camera was kept fairly zoomed out in order to (1) capture the full depth of the flow; and (2) cover a large streamwise extent ($\sim$1 m) with a minimal number of camera positions. As a result, the sublayer was resolved only in the low-stress region underneath the first crest of the jumps.

To illustrate this, recall the typical grid spacings discussed earlier. The first grid point above the flume bottom was typically at a height of about 0.75 mm. With a shear velocity of 4 cm s^{-1}, which was typical of the approach flows, the sublayer thickness is approximately 0.1 mm, which is far less than the grid resolution. Underneath the crests, where the shear is very low ($u^* \sim 0.5$ cm s^{-1}), the sublayer thickness is on the order of 1 mm. In these low stress regions, therefore,

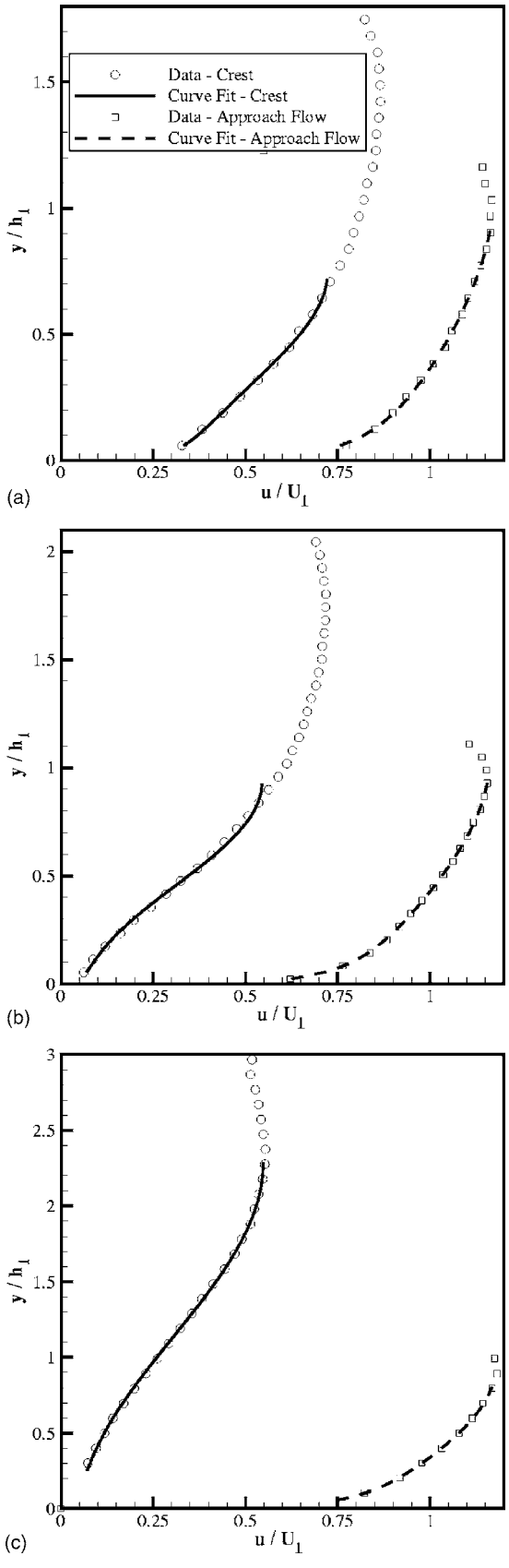

Fig. 12. Vertical mean velocity profiles in the supercritical approach flow and underneath the first crest. For clarity, only every other data point is shown. Also shown are the curve fits obtained with Cole's law: (a) Trial 1; (b) Trial 2; and (c) Trial 3.

Table 3. Boundary Shear Stress, in Supercritical Approach Flow and Beneath First Crest, Derived from Application of Coles' Law to Mean Vertical Velocity Profile

Trial	Approach τ_0 (Pa)	Crest τ_0 (Pa)
1	1.31	0.300
2	1.59	0.030
3	3.81	0.031

the PIV measurements of mean velocity should lead directly to the boundary stress.

Streamwise distributions of shear stress from the two methods are compared in Fig. 13 for all three trials. Also shown are the streamwise distributions of the elevation of the first grid point in wall units. Consider first the results obtained from the application of Coles' law and note that, in order to maximize the visual clarity near the origin of the vertical axis, the axis upper limits truncate the results in the supercritical approach flows. Next, note that the shear stress is inversely proportional to flow depth, with maximum values in the supercritical approach flows and minimum values beneath the crests of the jumps. In Trials 1 and 2, which are undular in nature, the shear rises as the flow accelerates through the trough following each crest. In Trials 2 and 3, the reduction in shear below the crest is particularly strong, with the observed shear nearly vanishing (recall Table 3).

When the results from the two methods are compared, Fig. 13 indicates a significant discrepancy over much of the extent of the jumps. From the preceding discussion, it is clear that this is due to the fact that the first available grid point from the PIV analysis generally lies outside of the viscous sublayer. As a result, shear stress derived from Eq. (5) and an assumed linear velocity profile will underestimate the shear, as the figure confirms. In low-shear regions, where the vertical position of the first grid point approaches ~10 wall units, however, the agreement between the two stress estimates is quite good. For the present experiments, these regions are limited to the first crests of the jumps. A higher magnification factor, through the use of a higher resolution camera or a smaller imaged area, will extend the range within which the stress can reliably be estimated with Eq. (5).

As a final point, the present shear stress results can be compared with those obtained by Chanson (2000) with a Preston tube. In particular, he presents data on the streamwise variation of centerline shear stress for a run with $F_1=1.48$, which is in proximity to Trial 1 of the present study. His measurements show that the shear stress underneath the first crest is 22% that of the supercritical approach flow. The present measurements, from Coles' law [Fig. 13(a)] show a value of 20%, which is in good agreement.

Concluding Remarks

PIV measurements of free undular and hydraulic jumps have been performed. For three different Froude numbers, ensembles of 400 image pairs at 10 different streamwise locations were tiled together into "mosaic" images of the jumps. Qualitatively, plots of

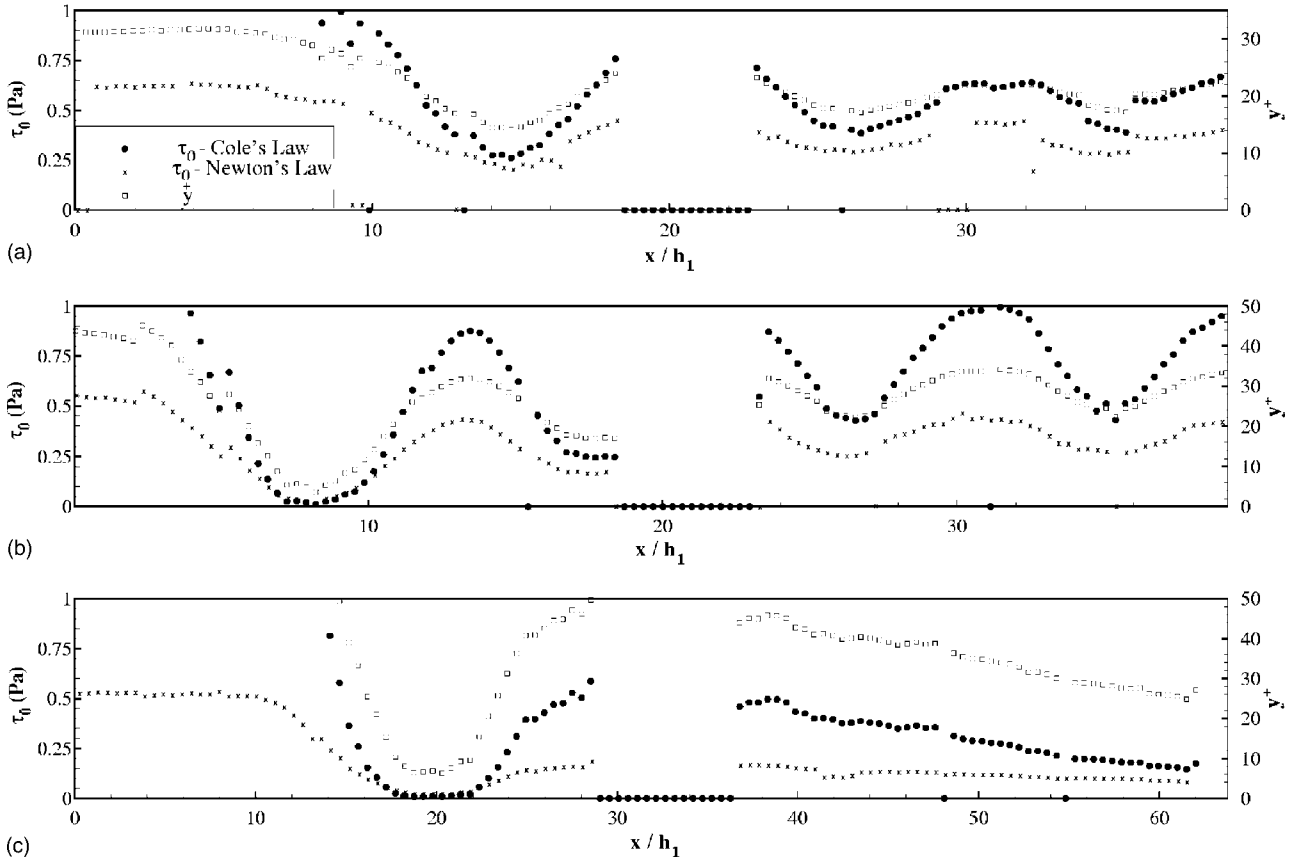

Fig. 13. Streamwise profiles of dimensional boundary shear stress, as determined from Newton's law of viscosity. Also shown are the shear stress profiles determined from Cole's law. Finally, the streamwise distributions of the elevation of the first grid point in wall units are shown: (a) Trial 1; (b) Trial 2; and (c) Trial 3.

mean variables such as velocity and vorticity yielded a highly resolved look at the kinematics inside these transitional flows. Only for the highest Froude number was a vortical roller detected.

Several methods for quantitatively determining the boundary shear stress from the PIV measurements were investigated. Of these, two proved capable of determining the boundary shear in regions other than the uniform supercritical approach flow. Coles' law of the wake was applied to vertical velocity profiles at all streamwise locations, yielding the distribution of boundary shear with streamwise distance. The boundary layer thickness, the shear velocity, and the wake parameter were all treated as smoothly varying functions of streamwise distance and were determined through constrained optimization.

The boundary stress was also determined directly from the fluid strain rate in the viscous sublayer. The success of this method relies upon the ability of the PIV measurements to resolve the sublayer. For the present experiments, this was possible only in the low-stress regions underneath the crests. By increasing the magnification and imaging a smaller field of view, PIV measurements will be able to determine the boundary stress at all streamwise locations using this approach.

The technical challenges associated with applying PIV to even stronger hydraulic jumps are significant. A high void fraction, due to the aeration at the roller, will obscure the optical path between the object and image planes. This will lead to blurry images and poor image correlations. If the emphasis is solely on boundary shear, high magnification imaging of the near-boundary region only will help to alleviate this difficulty, as the bubbles reside primarily in the upper regions of the flow.

Notation

The following symbols are used in this paper:

B = logarithmic velocity profile constant;
b = flume width;
D_h = hydraulic diameter;
$(D_u, D_v, \lambda_u, \lambda_v)$ = coefficients;
F_1 = supercritical Froude number;
f = friction factor;
h = general flow depth;
h_1 = supercritical flow depth;
R = Reynolds number;
U_1 = depth-averaged supercritical flow velocity;
(u, v) = streamwise and vertical velocity components;
(u', v') = horizontal and vertical velocity fluctuations;
u^* = shear velocity;
(x, y) = horizontal and vertical position;
δ = boundary layer thickness;
ϵ = roughness height;
η = scaled boundary layer coordinate;
κ = von Kármán constant;
ν = kinematic viscosity;
ξ = vorticity;
τ = shear stress;
Π = Cole's law wake parameter; and
τ_0 = boundary shear stress.

References

Chanson, H. (2000). "Boundary shear stress measurements in undular flows: Application to standing wave bed forms." *Water Resour. Res.*, 36(10), 3063–3076.

Chanson, H., and Brattberg, T., (2000). "Experimental study of the air-water shear flow in a hydraulic jump." *Int. J. Multiphase Flow*, 26, 583–607.

Chanson, H., and Montes, J., (1995). "Characteristics of undular hydraulic jumps: Experimental apparatus and flow patterns." *J. Hydraul. Eng.* 121(2), 129–144.

Chistensen, K., Soloff, S., and Adrian, R., (2000). "PIV Sleuth—Integrated acquisition, interrogation, and validation software for particle image velocimetry." *Rep. No. 943*, Dept. of Theoretical and Applied Mechanics, University of Illinois, Champaign, Ill.

Coles, D. (1956) "The law of the wake in the turbulent boundary layer." *J. Fluid Mech.*, 1, 191–226.

Hornung, H., Willert, C., and Turner, S. (1995). "The flow field downstream of a hydraulic jump." *J. Fluid Mech.*, 287, 299–316.

Kirkgoz, M., and Ardichoglu, M. (1997). "Velocity profiles of developing and developed open channel flow." *J. Hydraul. Eng.*, 123(12), 1099–1105.

Leutheusser, H., and Kartha, V. (1972). "Effects of inflow condition on hydraulic jumps." *J. Hydr. Div.*, 98(8), 1367–1385.

Liu, M., Rajaratnam, N., and Zhu, D. (2004). "Turbulence structure of hydraulic jumps of low Froude numbers." *J. Hydraul. Eng.*, 130(6), 511–520.

Long, D., Steffler, P., and Rajaratnam, N. (1990). "Lda study of flow structure in submerged hydraulic jump." *J. Hydraul. Res.*, 28(4), 437–460.

Misra, S., Kirby, J., Brocchini, M., Veron, F., Thomas, M., and Kambhamettu, C. (2005). "Hydraulic jump as a quasi-steady spilling breaker: An experimental study of similitude." *J. Fluid Mech.*, in press.

Montes, J., and Chanson, H. (1998). "Characteristics of undular hydraulic jumps: Experiments and analysis." *J. Hydraul. Eng.*, 124(2), 192–205.

Murzyn, F., Mouaze, D., and Chaplin, J. (2005). "Optical fibre probe measurements of bubbly flow in hydraulic jumps." *Int. J. Multiphase Flow*, 31, 141–154.

Nezu, I., and Rodi, W. (1986). "Open-channel flow measurements with a laser Doppler anemometer." *J. Hydraul. Eng.*, 1125(5), 335–355.

Ohtsu, I., Yasuda, Y., and Gotoh, H. (2001). "Hydraulic condition for undular-jump formations." *J. Hydraul. Res.*, 39(2), 203–209.

Ohtsu, I., Yasuda, Y., and Gotoh, H. (2003). "Flow conditions of undular hydraulic jumps in horizontal rectangular channels." *J. Hydraul. Eng.*, 129(12), 948–955.

Raffel, M., Willet, C., and Kompenhans, J. (1998). *Particle image velocimetry*, Springer, Berlin.

Rajaratnam, N. (1965). "The hydraulic jump as well jet." *J. Hydr. Div.*, 91(5), 107–134.

Resch, F., Leutheusser, H., and Alemum, S. (1974). "Bubbly two-phase flow in hydraulic jump." *J. Hydr. Div.*, 100(1), 137–149.

Rouse, H., Siao, T. T., and Nagaratnam, S. (1958). "Turbulence characteristics of the hydraulic jump." *J. Hydr. Div.*, 84(1), 1–30.

Schubauer, G., and Klebanoff, P. (1950). "Investigation of separation of the turbulent boundary layer." *Rep. No. 2133*, National Advisory Committee for Aeronautics, Washington, D.C.

Streinruck, H., Schneider, W., and Grillhofer, W. (2003). "A multiple scales analysis of the undular hydraulic jump in turbulent open channel flow." *Fluid Dyn. Res.*, 33, 41–55.

Svendsen, I., Veeramony, J., Bakunin, J., and Kirby, J. (2000). "The flow in weak turbulent hydraulic jumps." *J. Fluid Mech.*, 418, 25–57.

White, F. (1991). *Viscous fluid flow*, 2nd Ed., McGraw-Hill, New York.